Vortex nucleation in a mesoscopic Bose superfluid and breaking of the parity symmetry

D. Dagnino,[1] N. Barberán,[1] and M. Lewenstein[2,3]
[1]*Estructura i Constituents de la Matèria, Facultat de Física, Universitat de Barcelona, E-08028 Barcelona, Spain*
[2]*Institut de Ciències Fotòniques (ICFO), Parc Mediterrani de la Tecnologia, Spain*
[3]*Institució Catalana de Recerca i Estudis Avançats (ICREA), E-08010 Barcelona, Spain*
(Received 8 July 2009; published 13 November 2009)

We analyze vortex nucleation in mesoscopic two-dimensional Bose superfluid in a rotating trap. We explicitly include a weakly anisotropic stirring potential, breaking thus explicitly the axial symmetry. As the rotation frequency passes the critical value Ω_c, the system undergoes an extra symmetry change or breaking. Well below Ω_c, the ground state is properly described by the mean-field theory with an even condensate wave function. Well above Ω_c, the mean-field solution works also well, but the order parameter becomes odd. This phenomenon involves therefore a discrete parity symmetry breaking. In the critical region, the mean-field solutions exhibit dynamical instability. The true many-body state is a strongly correlated entangled state involving two macroscopically occupied modes (eigenstates of the single-particle density operator). We characterize this state in various aspects: (i) the eligibility for adiabatic evolution, (ii) its analytical approximation given by the maximally entangled combination of two single modes, and finally (iii) its appearance in particle detection measurements.

DOI: 10.1103/PhysRevA.80.053611 PACS number(s): 03.75.Hh, 03.75.Kk

I. INTRODUCTION

Symmetry changes or breaking belong to some of the most fascinating phenomena in nature. In classical physics, they are often associated with phase transitions in macroscopic systems [1,2]. Paradigm examples of symmetry breaking concern magnetic phenomena, such as, for instance, appearance of ferromagnets at temperatures lower than the Curie temperature, T_c. In the classical world, symmetry changes or breaking (C or B) are driven by thermal fluctuations and in the standard Landau-Ginzburg scenario are associated with increase of classical correlations and arousal of the long-range order. The mean-field approach, which goes back to "molecular-field theory" of Curie-Weiss [3], provides very often quite correct description of these phenomena away from criticality. Close to critical temperature, quantitative description requires the use of renormalization-group approach *à la* Wilson [4,5].

In quantum physics paradigm examples of symmetry C or B deal with low-temperature behavior of weakly interacting quantum Bose gases and Bose-Einstein condensation [6]. In the quantum world, particularly interesting are quantum phase transitions [7] and quantum symmetry C or B that are driven by quantum fluctuations. They can occur either at zero temperature or in quantum dynamical externally driven systems.

The symmetry C or B that have drawn a lot of attention since the early discovery of superfluids [8] until the recent studies of Bose-Einstein condensates (BECs) is nucleation of vortices in rotating superfluids. In fact, one of the most striking properties of superfluid and condensed systems is their response to rotation. The only way to acquire angular momentum is by the nucleation of vortices, topological singularities surrounded by condensed atoms revolving around their cores. The cores are well localized and have size of the, so-called, healing length. At low temperatures, they are empty, whereas at higher temperatures, they are filled with the thermal fraction of the condensate. For quantum gases, atoms are usually confined in an isotropic harmonic trap and experience an additional quadratic potential rotating at angular frequency Ω (for a review, see [9,10]). Standard textbooks [6] associate vortex nucleation with thermodynamic instability. When the rotation frequency is small, there exists a mean-field solution of the equation describing the BEC order parameter (condensate wave function) with a single vortex [11,12]; this solution has, however, larger (free) energy than the one corresponding to the condensate at rest [13]. Above certain critical rotation frequency, the solution with the vortex becomes a ground state and in principle may be achieved at low temperature being driven by thermal fluctuations. In practice, experiments with BEC occur in a completely different way. Typically, one prepares a condensate at very low temperature and then applies a certain dynamical perturbation to create a vortex. First, vortices have been created at JILA [14] using a kind of phase imprinting method [15]. It turned out, however, that the method consisting of slight deformation and rotation of the trap or, alternatively, "laser stirring" [16] was more efficient and led to numerous spectacular observations such as that of Abrikosov lattice [16–22] (for a review, see [9,23]).

BECs of dilute atomic gases offer particular possibilities for studies of nucleation of vortex states and their expansion in the course of time-of-flight (TOF) detection. In addition, these systems allow for experimental analysis and manipulation of mesoscopic confined clouds of condensed atoms trapped in the sites of optical lattices or in optical microtraps. This opens the perspective to compare directly results of exact numerical analysis for small systems to experiments and to different approximate calculations (for the first experiments in this direction, see [24,25]). Particularly interesting are the studies of the applicability of the mean-field (MF) theory within specific conditions. For confined systems at large rotation frequencies (in analogy to charged particles submitted to high magnetic fields), strongly correlated states develop: the so-called fractional quantum Hall (FQH)-type

states [10,26,27]. Such states cannot be described by a single-particle wave function that would play the role of an order parameter.

From a theoretical point of view, the vortex nucleation can be tackled by several techniques, ranging from a MF approach based on the Gross-Pitaevskii equation (GPE) [28–31] to the investigation of the many-body energy eigenstates [32–38]. Many authors addressed the question of vortex nucleation theoretically, asking in the first place for energetic stability of the vortex configuration as a ground state. Within the mean-field approach, this has been discussed mainly in the context of thermodynamic stability (cf. [6,13]). Several papers discussed, however, the case of $T=0$ and vortex nucleation in the ground state (GS) of the system using the exact quantum description (cf. [26,33,35,36,39]) or rigorous derivation of the MF equations [40,41]. More recent papers treated the problem of dynamics of vortex, or vortex lattice nucleation in elliptically deformed rotating traps, using mean-field method (i.e., time-dependent GPE [6]) and trying to reproduce the experimental results. The conclusion of these works is that vortex nucleation is inevitably associated to dynamical instability of the solutions of GPE [29,42]. Same results hold in the case of vortex nucleation via phase imprinting [43]. Some authors [30] claim that apart from the dynamical instability, a Landau instability (associated to dissipation) is also necessary to allow vortices to penetrate the BEC. The dynamical instability GPE is generically associated to the appearance of squeezing of two Bogoliubov–de Gennes (BdG) quasiparticle modes, i.e., exponentially growing two-mode entanglement in the regime of validity of BdG (i.e., regime of small Gaussian fluctuations around the MF solutions) [44]. This observation already indicates the necessity of going beyond the mean-field at the instability.

Much less is known about exact dynamics of the vortex nucleation. Parke *et al.* [38] considered recently this problem for a mesoscopic sample of atoms in the lowest Landau level (LLL) and discover striking non-mean-field effects in the (stationary) spectrum of the system at the critical rotation frequency Ω_c. They interpreted their results in terms of cooperative tunneling of a vortex pair by "requantizing" the mean-field theory (reduced to three relevant modes). In a recent paper [45], we used another approach and studied exact dynamics of a mesoscopic sample of atoms in a elliptically deformed rotating harmonic trap. Our main result was that as one increases Ω, at the Ω_c, the mean-field description ceases to be valid. The system enters a strongly correlated and entangled state, well described by an effective two-mode model. The mean-field description (similar to that of Ref. [38]) exhibits dynamical instability and hysteresis for $\Omega \simeq \Omega_c$. Since we explicitly include an anisotropic stirring potential, the present mechanism concerns a discrete parity symmetry breaking. Therefore, it differs from the case of the vortex nucleation in axially symmetric traps: in the latter case, breaking of the continuous rotational symmetry involves a gapless Nambu-Goldstone mode [46], while here we deal with a gapped system.

We believe that this example constitutes a paradigm of mean-field symmetry C or B in the course of adiabatic evolution of a many-body system. The character of the strongly correlated states depend on the nature and character of the symmetry C or B and the specific system—it is thus different in our case and in the case of Ueda and Nakajima [46], in the case of rotating lattice rings [47], or in BEC in a tilted double-well potential [48]. The last reference [48] reveals, however, a feature closely related to our results, which may have universal character: instability or chaotic behavior of the system predicted by the MF approach is a signature of the existence of a strongly correlated state.

This is quite an unexpected result, since at least for large systems, when N goes to infinity, the MF theory in the regime of nucleation of the first vortex where the angular momentum of the systems changes from $L=0$ to N is believed to be correct. This belief has been in fact recently supported by rigorous results in Ref. [41], where it has been proved that the MF expressions for the total energy of the system coincides with the exact result for large N. Moreover, while the MF description of the GS is not correct for moderately big N at criticality, the single-particle density is another example of a quantity correctly described by the MF approach. This last observation is supported by our result: we obtain that the density of the ground state at Ω_c for increasing N becomes indistinguishable from that obtained for small N. This means that some macroscopic mean quantities, such as the density or the total energy, are practically insensitive to the symmetry C or B process at criticality.

The aim of the present work is to perform a deeper analysis of the precursor state of the nucleation process, named Ψ_c from now on, using various techniques. First, we analyze the dynamical process of increasing rotation frequency and show that, during the time evolution from an initial GS at a starting rotation frequency (where the angular momentum is $L=0$) to the final one-vortex state where $L=N$, one must pass through a state that cannot be described by a MF order parameter. This state contains two macro-occupied modes of different parities of the single-particle density matrix. Second, we characterize this noncondensed state and its properties and ask how does this state exhibit these properties in measurement process. We note that similar questions have been posed in the context of appearance of the relative phase in the interference of two BECs in the course of measurements [49–51]. Inspired by the work of Javanainen and Yoo [49], we simulate the measurement process in a TOF experiment for a one-shot event and for the accumulation of a large number of single shots. To be able to perform the measurement simulation of the Ψ_c state assuming a large number of particles, we use a two-mode model which provides a very accurate approximation of the exact state. For most of the times, the single shot events produce a single vortex located randomly along the x axis whereas the accumulation of a large number of shots reproduce the density. We discuss the interpretation of the outcomes and relate them with other strongly correlated states discussed previously in various systems. Note that in the view of the recent experimental progress in detection of density of atomic clouds at a single atom level [52,53], our measurement simulation results could be directly observed in experiments proposed by us.

Our paper is organized as follows. In Sec. II, we present our model and a brief repetition of previous results for rotating bosonic systems. In Sec. III, we analyze the time evolution of the nucleation process. First, we look at the possibil-

ity of adiabatic evolution and second, we discuss a two-mode model for the GS at a critical frequency at which parity symmetry breaking takes place at the MF level. In Sec. IV, we study the energy spectrum as a function of the rotation frequency in terms of the contributions of different L subspaces in the GS and analyze the robustness of the Ψ_c state. In Sec. V, we describe measurement simulations and discuss their possible interpretations. Here, the comparison to a model cat state (analogous to that predicted in Ref. [47]) is included. Finally, in Sec. VI, we present our conclusions.

II. MODEL AND BACKGROUND

We assume a two-dimensional cloud of few condensed Bose atoms of mass M interacting via contact forces confined in a symmetric parabolic trap with frequency $\omega_\perp$. Two extra perturbing potentials are also considered. One simulates a stirring laser that sets the system in rotation by a slight anisotropic deformation in the xy plane, rotating at angular frequency Ω around the z axis breaking the cylindrical symmetry. The second one is a perturbation that breaks the parity symmetry, a symmetry that is otherwise preserved by the previous terms. The last one simulates possible second-order contributions of the laser fields and will help us in the analysis of the system. The rotation frequency Ω is strong enough to assume the LLL regime [39], i.e., we consider that the kinetic energy within the LLL given by $\hbar(\omega_\perp - \Omega)$, the strength of the interaction, and both perturbations are small compared to the separation between Landau levels given by $\hbar(\omega_\perp + \Omega)$ [54]. It is implicit in our model that in the z direction, a strong parabolic trap of frequency ω_z freezes the atomic motion producing an effective two-dimensional (2D) system. We model the contact interaction U and the two perturbing potentials V_1 and V_2 by

$$U(\vec{r}_i,\vec{r}_j) = (\hbar^2 g/M)\sum_{i<j}^{N} \delta(\vec{r}_i - \vec{r}_j), \tag{1}$$

$$V_1(\vec{r}) = 2AM\omega_\perp^2 \sum_i^N (x_i^2 - y_i^2), \tag{2}$$

and

$$V_2(x) = B\frac{M\omega_\perp^2}{\lambda_\perp}\sum_i^N x_i^3, \tag{3}$$

where $g=\sqrt{8\pi}a/\lambda_z$, a being the three-dimensional (3D) scattering length, $\lambda_z=\sqrt{\hbar/M\omega_z}$, and $\lambda_\perp=\sqrt{\hbar/M\omega_\perp}$. The dimensionless parameters g, A, and B measure the strength of each term. We choose $\lambda_\perp$, $\hbar\omega_\perp$, and $\omega_\perp$ as units of length, energy, and frequency, respectively. It is worth mentioning that a simpler term that breaks the parity symmetry $\sim B\Sigma_i x_i$ is a center-of-mass excitation that would leave the internal structure unchanged revealing no new physics. In the second-quantized formalism, the Hamiltonian of the system projected onto the LLL in the rotating reference frame is described by

$$\hat{H} = \alpha\hat{L} + \beta\hat{N} + \hat{U} + \hat{V}_1 + \hat{V}_2 \equiv \hat{H}_0 + \hat{U} + \hat{V}_1 + \hat{V}_2, \tag{4}$$

where $\alpha=\hbar(\omega_\perp-\Omega)$ and $\beta=\hbar\omega_\perp$. $\hbar\hat{L}$ and $\hat{N}$ are the total z-component angular momentum and particle number operators, respectively; H_0 being the kinetic contribution. The contact-interaction term is given by the operator

$$\hat{U} = \frac{1}{2}\sum_{m_1m_2m_3m_4} U_{1234} a_{m_1}^\dagger a_{m_2}^\dagger a_{m_4} a_{m_3}, \tag{5}$$

where the matrix elements read

$$U_{1234} = \langle m_1 m_2|U|m_3 m_4\rangle = \frac{g}{\lambda_\perp^2\pi}\frac{\delta_{m_1+m_2,m_3+m_4}}{\sqrt{m_1!\,m_2!\,m_3!\,m_4!}}\frac{(m_1+m_2)!}{2^{m_1+m_2+1}}. \tag{6}$$

The operators $a_{m_i}^\dagger$ and a_{m_i} create and annihilate a boson in a single-particle eigenstate of $\hat{H}_0$ with angular momentum m_i, respectively. These eigenstates are taken as a basis to represent wave functions and operators in the second-quantized formalism. We will refer to this set of functions as the Fock-Darwin (FD) functions restricted to the LLL (without nodes in the radial direction) and will denote them as $\varphi_m=\frac{1}{\sqrt{\pi m!}}(x+iy)^m\exp[-(x^2+y^2)/2\lambda_\perp^2]$, being m its angular momentum. The term $\hat{V}_1$ in Eq. (4) is given by

$$\hat{V}_1 = \frac{A}{2}\sum_m \sqrt{m(m-1)}a_m^\dagger a_{m-2} + \sqrt{(m+1)(m+2)}a_m^\dagger a_{m+2} \tag{7}$$

and the term $\hat{V}_2$ by

$$\hat{V}_2 = \frac{B}{8}\sum_m [\sqrt{m(m-1)(m-2)}a_m^\dagger a_{m-3} + 3(m+1)\sqrt{m}a_m^\dagger a_{m-1} + 3(m+2)\sqrt{m+1}a_m^\dagger a_{m+1} + \sqrt{(m+1)(m+2)(m+3)}a_m^\dagger a_{m+3}]. \tag{8}$$

In the absence of anisotropy ($A=B=0$), the total angular momentum of the GS as a function of Ω shows sharp steps at critical values Ω_i $i=1,2\ldots$, being Ω_1 ($\Omega_1=\omega_\perp-gN/8\pi$) the value at which the angular momentum of the system jumps from zero to $L=N$ for all N. Above Ω_1, a plateau indicating constant angular momentum extends up to Ω_2 where the second jump, not always to $L=2N$, takes place. From this value, a sequence of jumps and plateaus emerges up to the last possible L value given by $L=N(N-1)$, corresponding to the Laughlin state. The extension of the first plateau, from Ω_1 to Ω_2, increases with N and at the same time, Ω_1 decreases (this is a characteristic of the first plateau; in contrast, the next ones reduce drastically as N increases). From the expression of Ω_1, it is evident that for a given value of g, there is a maximum number of atoms compatible with our LLL assumption; for large N ($N\geq 25$ for $g=1$), the functional relation between Ω_1 and N cannot be linear anymore; extra Landau levels must be taken into account.

Eigenstates with more than one vortex can only exist locally at Ω_i where several eigenfunctions with different angular momentum but degenerated in energy can be combined to

generate vortex configurations in a spontaneous symmetry-breaking mechanism. For instance, for $N=5$, there is degeneracy between the states with $L=0$, 2, 3, 4, and 5 at Ω_1, $L=5$ and 8 at Ω_2, or $L=8$, 10, and 12 at Ω_3. Namely, for small systems, the possibility to have vortex states is localized around discrete values of Ω. However, for larger N, on one hand, the distance between the critical values of Ω_i is drastically reduced [36] and on the other hand, the steps are softened due to the slight anisotropy that must be applied to accelerate the system; these two effects effectively provide the possibility to nucleate vortices in a continuous way for all $\Omega > \Omega_1$ [17,40].

If anisotropy is included in the Hamiltonian, the steps are softened. For a fixed A (and $B=0$), the softening is larger for small values of N in such a way that the steps may disappear. This effect can be reduced increasing g, namely, the increase of anisotropy reduces the effect of the interaction. To keep a well defined first step around the same Ω_1 for all N, we considered $gN=$const in our calculations; in addition, this decrease of the interaction as N increases preserves the LLL condition [39].

Having specified the Hamiltonian of the model, we perform exact diagonalization. The isotropic Hamiltonian can be diagonalized in boxes of finite L subspaces whereas, in the anisotropic case, several basis of different L subspaces must be considered until convergence is obtained, depending on the value of A and B. However, if $B=0$ since the term $\hat{V}_1$ in Eq. (7) can only mix L and $L \pm 2$, the parity of the angular momentum is well defined and only subspaces with the same parity must be considered.

To finish this section, we must introduce the single-particle density-matrix (SPDM) operator and its eigenfunctions as tools to be used in the next sections. One of our aims is to analyze the states generated as Ω grows in a dynamical process that follows the evolution of the GS from an initial value Ω_0 (smaller than a critical frequency Ω_c to be defined later) to a final value $\Omega_f > \Omega_c$ at the middle of the first plateau, where the first vortex has been nucleated. For these relatively low values of Ω and far from the critical frequency, the degree of condensation is high and the eigenfunction (a single-particle wave function) of the SPDM that corresponds to the highest occupation plays the role of the order parameter (OP) of the condensate [55]. To obtain this OP, we solve the eigenvalue equation for the SPDM

$$\int d\vec{r}' n^{(1)}(\vec{r},\vec{r}')\psi_k^*(\vec{r}') = n_k \psi_k(\vec{r}), \tag{9}$$

where

$$n^{(1)}(\vec{r},\vec{r}') = \langle \mathrm{GS}|\hat{\Psi}^\dagger(\vec{r})\hat{\Psi}(\vec{r}')|\mathrm{GS}\rangle, \tag{10}$$

with $\hat{\Psi}$ being the field operator. If there exist a relevant eigenvalue $n_1 \gg n_k$ for $k=2,3,\ldots$, then

$$\sqrt{n_1}\psi_1(\vec{r}) \tag{11}$$

plays the role of the OP of the system. The map of the local phase of this complex function gives precise information of the position of vortices [55]. The change of the phase by $2\pi\nu$ around a point, where ν is a positive integer, signals the location of a vortex with ν quanta of circulation. Notice that m labels the single-particle angular momentum from $m=0,1,2,\ldots$ of the FD functions, whereas $k=1,2,\ldots$ is a label that distinguishes between the eigenstates of the SPDM. In Appendix A, we show a detail derivation of the relationship between the operators that create FD functions $\hat{a}_m^\dagger$ and those that create eigenfunctions of the SPDM operator $\hat{b}_k^\dagger$.

III. DYNAMICS OF THE NUCLEATION OF THE FIRST VORTEX

A. Adiabatic evolution

First, we try to find out if the nucleation of the first vortex can be obtained as the final configuration of the adiabatic time evolution of the initial GS submitted to increasing Ω. To understand how the resulting state changes during the process, we perform several runs from Ω_0 to Ω_f for increasing time intervals and compare the results to the sequence of stationary solutions obtained from the diagonalization of the time-independent Hamiltonian for the same range of Ω values.

Assuming linear dependence in time of the rotation frequency as

$$\Omega(t) = \Omega_0 + \gamma t, \tag{12}$$

where γ is a constant, we solve the Schrödinger equation

$$i\partial_t|\Phi(t)\rangle = \hat{H}(t)|\Phi(t)\rangle \tag{13}$$

for the initial exact solution $|\Phi(t=0)\rangle$ at Ω_0. If we assume the expansion of the state in the Fock basis as $|\Phi(t)\rangle = \Sigma_k c_k(t)|k\rangle$, where $|k\rangle$ is the N-particle Fock state with the well-defined angular momentum, and project Eq. (13) on the state $|j\rangle$, we obtain the system of equations

$$i\partial_t c_j(t) = \sum_k c_k(t)\langle j|\hat{H}(t)|k\rangle, \tag{14}$$

which can be solved numerically. The bracket $\langle j|\hat{H}(t)|k\rangle$ is expressed as

$$\langle j|\hat{H}(t)|k\rangle = \langle j|\hat{H}_1|k\rangle + L_j[1-\Omega(t)]\delta_{jk}, \tag{15}$$

with a time-independent matrix which must be calculated only once, plus a time-dependent diagonal term. $\hat{H}_1 = \beta\hat{N} + \hat{U} + \hat{V}_1 + \hat{V}_2$; L_j is here the angular momentum of the N-particle Fock state $|j\rangle$.

We compare then the time evolution to the corresponding sequence of stationary states at instant rotation frequencies and choose three different criteria of adiabaticity. The first one compares the profiles of the angular momentum as a function of Ω. We consider that adiabaticity is obtained when the maximum difference between the curves is 0.03. In Fig. 1, we plot for $N=6$ ($A=0.03$ and $B=0$) the evolution of the angular momentum of the state that fulfils the condition of being the exact GS at $\Omega_0=0.4$, up to $\Omega_f=0.85$ at the middle of the first plateau. Different time intervals Δt have been considered until adiabaticity is achieved for $\Delta t=30\,000$; the black line corresponds to the stationary solutions. This

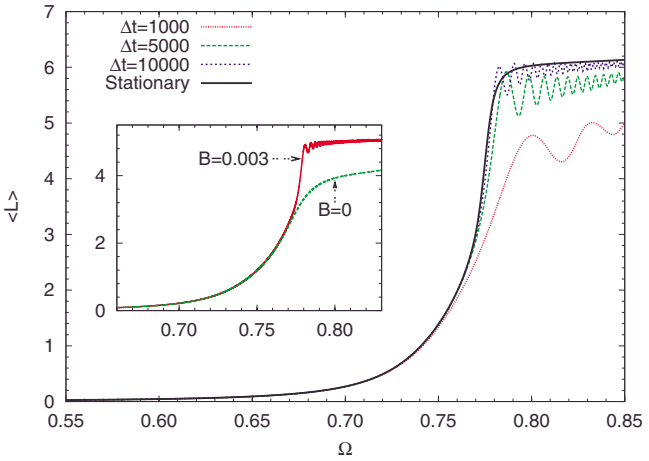

FIG. 1. (Color online) For $N=6$ and $B=0$, time evolution of the mean value of the angular momentum (in units of $\hbar$), taking as the initial condition its GS value at $\Omega_0=0.4$ (not shown in the figure). The value of Δt is the time used in the process to run linearly from Ω_0 to $\Omega_f=0.85$ in units of $\omega_\perp^{-1}$. For $N=5$, inset shows $\langle L\rangle$ over Ω; for $B=0$ once adiabaticity is fulfilled and close to adiabaticity for $B=0.003$. $\Delta t=50\,000$ in the last case. ($A=0.03$ and $g=1$ have been considered.)

means that from the stationary state at $\Omega_0=0.4$, a slow evolution taking at least 28 s is necessary to nucleate the first vortex at Ω_f evolving through stationary states ($g=1$, $A=0.03$, and $\omega_\perp=2\pi\times 175$ Hz has been considered). The equilibrium state at $\Omega_0=0.4$ can be experimentally realized after relaxation once the system is suddenly put in rotation at $\Omega=0.4$ [16]. The origin of the oscillations can be clarified by the analysis of the contributions of different L subspaces in the expansion of $|\Phi(t)\rangle$ as Ω evolves. Figure 2 shows the weight of each subspace within $\Phi(t)$. It can be inferred that the interplay between $L=6$ and $L=4$ produces the oscillations. We proved that this is a general result for all N; very fast evolution is possible, keeping adiabaticity, from Ω_0 up to about Ω_1, whereas beyond this frequency, a sequence of quadrupolar excitations between $L=N$ and $N-2$ produces oscillations on $\langle L\rangle$ lowering the speed.

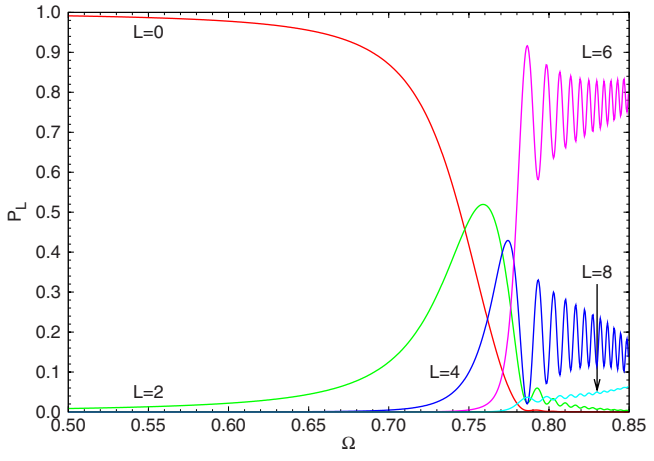

FIG. 2. (Color online) Evolution of the weight (P_L) of the L-subspace components within $\Phi(t)$ before adiabaticity for $N=6$, $g=1$, $A=0.03$, and $B=0$.

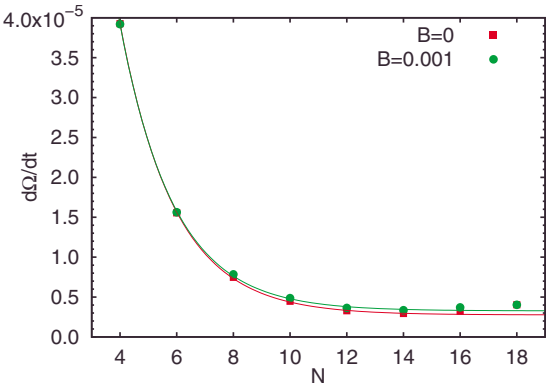

FIG. 3. (Color online) Dependence on N of γ_c, the critical value of the variation of Ω with time, necessary to arrive to adiabaticity. $B=0$ and $B=0.001$ have been considered for the lower and upper curves, respectively; $A=0.01$ and $gN=6$ in both cases.

A similar behavior is found for our second criterion based on the evolution of the expected value of the energy. In contrast to the previous case, however, the coincidence with the stationary values is obtained much faster (about $\Delta t=5000$ for the GS), producing the incorrect impression of adiabaticity—incorrect since other characteristics of the system, as is the case of the angular momentum, are still not reproduced.

Finally, the third option is to measure the overlap between the exact GS and $|\Phi(t)\rangle$ at Ω_f and to consider that one gets adiabaticity when the overlap is larger than 0.99. For $N=6$, adiabaticity is fulfilled in 21 s, compatible with the result obtained from the first criterion.

For odd values of N, the time evolution driven by a parity-preserving Hamiltonian (with $B=0$) cannot carry up $\langle L\rangle$ from 0 to N and a slight perturbation, which breaks parity symmetry, is necessary. In other words, the sequence of stationary solutions of the parity-invariant Hamiltonian develop a first-order transition at about Ω_1 where even L-subspace contributions are substituted by the odd ones within the composition of the GS. In the inset of Fig. 1, we show, for comparison, for $N=5$ the time evolution for the case when adiabaticity is achieved for $B=0$ and nearly achieved for $B=0.003$ ($\Delta t=50\,000$ in the last case). In the first case, the expected value of the angular momentum is around 4 and no vortex is nucleated, whereas in the second case, a one-vortex state with $\langle L\rangle=5$ is obtained.

Figure 3 shows γ_c defined as $\Omega_f=\Omega_0+\gamma_c\Delta t$ as a function of N. For fixed values of the initial and final frequencies taken for all cases at $\Omega_0=0.4$ and $\Omega_f=0.85$, we increase Δt until adiabaticity is fulfilled (using the third criterion previously mentioned) and from it, we obtain γ_c. In both cases, with and without the parity-breaking term in the Hamiltonian, γ_c converges, meaning that even for large number of particles, the process is possible at a finite time interval.

B. Two-mode state

To analyze the evolution of the GS in more detail (we focus on the case $B=0$), we look at the eigenfunctions of the SPDM [see Eq. (9)] and their occupations n_k. They provide an alternative representation of multiparticle states and op-

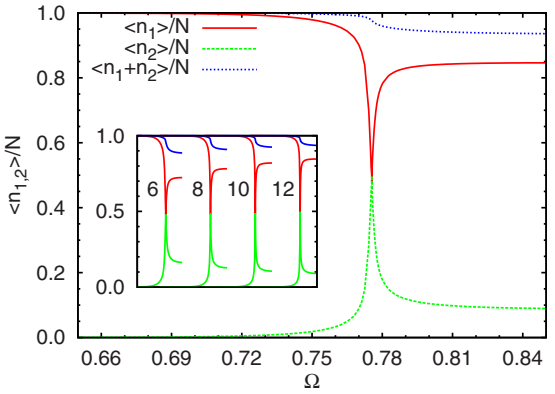

FIG. 4. (Color online) Evolution of the mean value of the occupations n_1/N and n_2/N in the GS, as a function of Ω, once adiabaticity is fulfilled for $N=12$. The peaks touch at $\Omega_c=0.7759$. The additions of both contributions are also shown. Inset shows the results for different number of particles. As N increases, the condensation far from Ω_c increases and at the critical frequency, the value of $n_{1,2}$ is closer to 0.5, meaning that the two-mode model is indeed better. The graphs are horizontally shifted for clarity. $A=0.03$ and $gN=6$ have been considered in all cases.

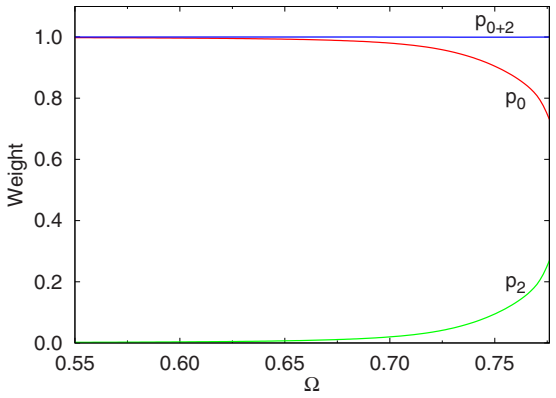

FIG. 5. (Color online) Weight vs Ω of the FD functions φ_0 and φ_2 (p_0 and p_2) in the expansion of the most occupied wave function ψ_1, below Ω_c, as well as their joint contribution. $A=0.03$ and $gN=6$ ($N=12$) have been considered.

erators by the substitution of the FD functions φ_m by ψ_k. The result obtained is that during the whole time evolution from Ω_0 to Ω_f, only two of these single-particle eigenstates, ψ_1 and ψ_2 (the most occupied and the next one), with occupations n_1 and n_2, respectively, play a role in the GS. Moreover, through the whole evolution $(n_1+n_2)/N \geq 0.9$ and as N increases, this joint occupation is even larger. In Fig. 4, the adiabatic change in time of the first two occupations n_k is shown. This result strongly suggests the substitution of the GS by a two-mode state in which only ψ_1 and ψ_2 are considered. We define as "critical" (Ω_c) the frequency where the coincidence of the occupations n_1 and n_2 takes place. The decrease of the anisotropy A reduces the width of the critical regime, but the peaks in the population of ψ_1 and ψ_2 always touch each other.

In contrast, if $B \neq 0$, n_1 is strictly greater than n_2 at Ω_c and although these modes are still the dominant ones, the peaks do not touch at any frequency. The two-mode model works well, but the system becomes slightly more condensed. However, within the region around Ω_c, the system lies always beyond the regime of applicability of MF theories [45].

Another relevant information is that only the three first LLL single-particle states (for $m=0,1,2$) have a significant weight in the expansion of ψ_1 or ψ_2. Below Ω_c, ψ_1 is a combination of φ_0 and φ_2; at Ω_c it changes its nature to a state that contains only the φ_1 and remains as that up to Ω_f. The second most occupied state, ψ_2, develops the opposite changes in such a way that they interchange their composition at the critical frequency. As a consequence, the density of the GS shows predominantly two symmetric vortices, produced by the combination of φ_0 and φ_2, that move from the edge to the center (up to a nonzero shortest distance) as Ω approaches Ω_c and a single centered vortex produced by φ_1 from Ω_c to Ω_f. Figure 5 shows the evolution of the weights (p_0 and p_2) of the FD functions in the expansion of ψ_1 up to the critical frequency where they disappear. Close to Ω_0, ψ_1 is essentially φ_0 (and ψ_1 is essentially the GS), producing a fully condensed state. Just before Ω_c, it has both components with significant weights and at Ω_c, these weights are substituted by the weight of the unique component φ_1 (not shown in the figure).

Had we considered the combination of φ_0 and φ_2 for the whole range from Ω_0 to Ω larger than $\omega_\perp$ (with the addition of a quartic potential), in the spirit of a MF approach, then the curves p_0 and p_2 in Fig. 5 would cross each other and would end with final values of $p_2=1$ and $p_0=0$ at some Ω, meaning that a single double-quantized vortex would be produced at the center of the condensate, in agreement with the results obtained by Saito and Ueda [56]. The evolution would not fulfill the condition of adiabaticity and the last state would be an excited state.

In order to perform simulations of TOF experiments in Sec. V, assuming a large number of particles to have good statistics, we combine the results from exact diagonalization with the use a two-mode model in the following way: at Ω_c, we analyze the overlap between the exact GS and N-body two-mode Fock states of the type

$$|n_1,n_2,0,0,\ldots\rangle, \tag{16}$$

where $n_1+n_2=N$, which will be abbreviated as $|n_1,n_2\rangle$. Here, we must clarify a point concerning the definition of ψ_1 and ψ_2. At Ω_c, $n_1=n_2$ and the "most occupied" state can be both of them. As long as we concentrate in the analysis of the GS at Ω_c, we choose for ψ_1 the expansion in terms of φ_0 and φ_2 and for ψ_2 the one represented by φ_1.

Figure 6(a) shows $|\langle \mathrm{GS}|n,N-n\rangle|^2$ as a function of n for $B=0$. The result means that in the GS, there is a nearly uniform distribution among the different components (better as N increases) and in addition, that $|\mathrm{GS}\rangle$ is very close to the maximally entangled (ME) state constructed from even n values, since the overlap $|\langle \mathrm{ME}|\mathrm{GS}\rangle|=0.92$ is indeed large. Here $|\mathrm{ME}\rangle$ is defined as

$$|\mathrm{ME}\rangle = [|N,0\rangle + |N-2,2\rangle + \cdots + |0,N\rangle]/\sqrt{N/2+1}. \tag{17}$$

Note that the combination $\Phi=\Sigma_{k=0}^{N}\sqrt{\binom{N}{k}}\alpha^{N-k}\beta^k|N-k,k\rangle$ for a given α and β is a condensate, a system with a single one-

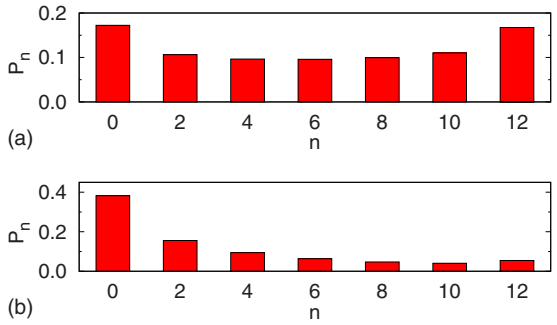

FIG. 6. (Color online) Analysis of the GS for $N=12$ at the critical frequency in terms of the square of the scalar products, $P_n = |\langle \mathrm{GS}|n,N-n\rangle|^2$. (a) is for $B=0$ and (b) for $B=0.001$. $|\langle \mathrm{ME}|\mathrm{GS}\rangle| = 0.92$ for $B=0$ and $|\langle \mathrm{PB}|\mathrm{GS}\rangle| = 0.840$ for $B=0.001$. $A=0.03$ and $gN=6$ ($N=12$) in both cases.

body wave function occupied: $\tilde{\phi}=\alpha\phi_1+\beta\phi_2$ since $\tilde{\phi}\otimes\tilde{\phi}\otimes\cdots\otimes\tilde{\phi}=\Phi$. However, there does not exist neither a pair α, β, that reproduces the state (17) with only even entries, nor a pair that reproduces the cat state [57]. Note also that we are using here the concept of entanglement for identical particles corresponding to the mode entanglement (for various ways of defining entanglement in systems of identical particles, see [58,59]). This analytic approximation to the GS allows us to simulate experimental TOF measurements with an arbitrarily large number of atoms, where the only ingredients supplied by the exact analysis are the coefficients of the expansions of ψ_1 and ψ_2 on the FD functions. We use it in Sec. V.

Figure 6(b) shows similar results for $B\neq 0$. The main difference between the two cases consists on the expansion of ψ_1 and ψ_2 in the FD states. In the parity-broken case, in both expansions, φ_0, φ_1, and φ_2 are significant. The decrease of the columns with n is exponential and can be accurately adjusted by an analytical function. We define as $|\mathrm{PB}\rangle$ (PB for parity broken) the expansion on $|n,N-n\rangle$ states with the appropriate decreasing coefficients. It must be pointed out that the single-particle odd occupations must be zero for $B=0$ and very close to it for $B=0.001$ not observable in the scale of Fig. 6(b). The variation of the weights for different number of particles converges as N increases, as shown in Fig. 7 where the results from $N=16$ and $N=18$ coincide. In Sec. V, we use the converged coefficient to simulate the measurements. For a given N, the distribution of weights shown in Fig. 6 is robust against changes in the anisotropy strength A.

For comparison, we also analyzed, for $B=0$, the overlap of the GS with other celebrated states. One is the "cat state" represented by the combination $|N,0\rangle+|0,N\rangle$ [47], which means that as a result of a single shot, the system can only appear as a full condensed state of each type with a probability of 50%; similar phenomenology was analyzed in Ref. [61] related with optical vortex cat states. Another is the so-called "fragmented state" with only one component in its expansion, given by $|N/2,N/2\rangle$ with a 50% of occupation for each mode [51], and the last case considered is the full condensed state. In Fig. 8, for $N=12$, we show the overlaps as a function of Ω for each case; the system evolves from a full condensed state at Ω_0 to a quite condensed one at Ω_f, passing through a strongly correlated state, very similar to $|\mathrm{ME}\rangle$ at the critical frequency.

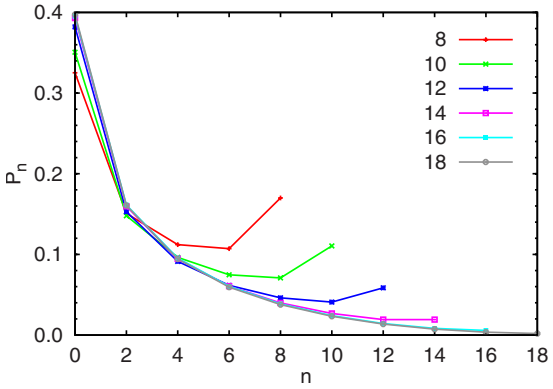

FIG. 7. (Color online) P_n (defined in the caption for Fig. 6) vs n for different number of atoms for ($B=0.001$). The cases $N=16$ and $N=18$ coincide and the result converges for larger N. For $N=18$, $|\langle \mathrm{PB}|\mathrm{GS}\rangle| = 0.700$. $A=0.03$ and $gN=6$ have been considered in all cases.

IV. ENERGY SPECTRUM

In Sec. III, we addressed the question related to the possibility of adiabatic evolution from Ω_0 to Ω_f in a finite Δt when nonzero values of A and B are included in the Hamiltonian. The conclusion was that as long as B is small compared to A and g, even for a large number of particles, Δt remains finite. In this section, in contrast, we analyze the energy gap between the GS and the first-excited state as a necessary ingredient, aside from the critical γ_c already treated in Sec. III, to decide if the adiabatic criterion is fulfilled. We look for the possibility of excitations of different multipolarity. First, we analyze the energy gap between the GS and the lowest-excited states during the evolution in terms of the contribution of the L subspaces in their composition and see how this analysis depends on A, B, and N. Next, we concentrate on the robustness of the GS of the parity-invariant Hamiltonian at the critical frequency against

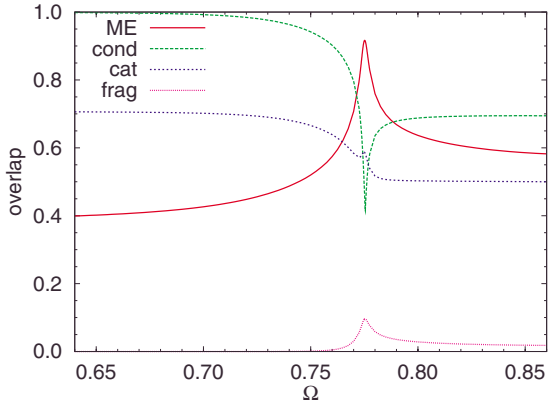

FIG. 8. (Color online) Overlaps, $|\langle \mathrm{St}|\mathrm{GS}\rangle|$ as a function of Ω, of the GS over different states (St): the maximum entangled (ME), the fully condensed (cond), the cat state (cat), and the fragmented state (frag) for $A=0.03$, $B=0$, and $gN=6$ ($N=12$).

occasional external perturbations, i.e., we inquire about the experimental feasibility of obtaining the Ψ_c state in the laboratory. This question is suggested by possible applications to quantum information, where it is necessary to manipulate and control the system.

For the symmetric Hamiltonian ($A=B=0$), as was mentioned in Sec. II, at the critical frequency ($\Omega_c=\Omega_1=\omega_\perp - gN/8\pi$ in this case), N stationary states are energy degenerated (those with $L=0$ and $L=2,\ldots,N$) as expected from the analytical expression of the energies

$$E_L = \frac{g}{4\pi}N\left(N-\frac{L}{2}-1\right)+(\omega_\perp-\Omega)L+N\omega_\perp$$
$$= L\left(\omega_\perp-\Omega-\frac{gN}{8\pi}\right)+\frac{gN}{4\pi}(N-1)+N\omega_\perp, \qquad (18)$$

which become L independent when $\Omega=\Omega_1$. This degeneracy is lifted by the introduction of nonzero A, B, or both. Figure 9 shows for $N=6$ the evolution of the energy spectrum for $A=B=0$, $A\neq 0$, and $B=0$, and $A=0$ and $B\neq 0$, respectively. In the second case, the energies are grouped in pairs of different parity, as was previously obtained by Parke *et al.* [38], namely, for some values of Ω, the lowest-excited state is nearly twofold degenerated being, however, well separated from the GS. This was the general trend in all considered cases ($N\leq 20$). As Ω changes, some crossings and anticrossings take place in such a way that the minimum gap between the GS and the first excitation (defined as G_m) may imply jumps from even to even (which is the case of $N\leq 6$) or even to odd (for $N>6$).

In Fig. 10, we show, for $N=10$, the evolution of the contributions of different L subspaces to the GS (upper figure) and to the first-excited state (bottom figure). We consider $A=0.03$ and a relatively large value of $B=0.005$ to emphasize the broken-parity effect. Since both symmetries are broken, all L subspaces have nonzero contributions. However, there is a remarkable difference between the regions below and above $\Omega_1=0.76$. For $\Omega<\Omega_1$, only even values of L are significant in spite of the fact that the Hamiltonian breaks parity symmetry and the presence of external fluctuations that would produce monopolar ($L\pm 1$) or octupolar ($L\pm 3$) excitations is irrelevant, since these excitations are energetically blocked; the most probable process is a quadrupolar excitation from $L=0$ to $L=2$. In contrast, for $\Omega>\Omega_1$, all even and odd values of L play a role; in particular, far from Ω_1, the change from $L=10$ to $L=9$ is the most probable scenario, which means that the possible nonadiabaticity of the evolution would be dominated by a *braking* process (i.e., slowing down the rotational speed of the system), where in an effective way, one of the atoms jumps from the condensed to the thermal phase, ceasing its contribution to the total angular momentum of the system. Had we suppressed B in Fig. 10, we would obtain for the first-excited state separated regions with only even or only odd contributions (due to crossings in the spectrum).

Finally, in Fig. 11, we show the minimal gap G_m as a function of N obtained from the parity-invariant Hamiltonian. We distinguish between two cases: in the upper curve

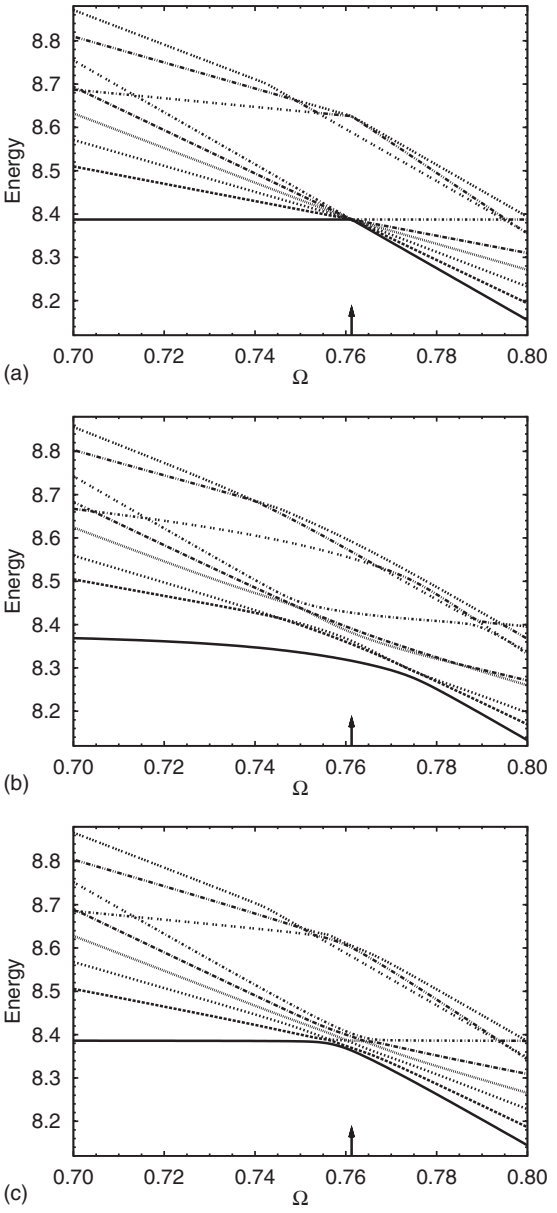

FIG. 9. Lowest contributions to the energy spectrum as a function of Ω for $N=6$ and $g=1$. In (a) we consider $A=B=0$, in (b) $A=0.03$ and $B=0$, and in (c) $A=0$ and $B=0.01$, respectively. The arrow marks the value of Ω_1.

(2×2), only even values of L are considered, i.e., it gives the gap for quadrupolar excitations, in contrast, in the lower branch, all L values are considered (1×1) and it represents the minimal gap that must be overcome by any perturbation of arbitrary multipolarity. If the system is protected against parity-breaking perturbations, the adiabaticity of the process is guaranteed (upper curve) since G_m tends to a constant for large N and simultaneously γ_c decreases in such a way that the adiabatic criterion given by $\gamma_c N/G_m \ll 1$ is fulfilled (for example, 0.006 for $N=10$). However, if parity-breaking excitations can occur and the number of particles is large, the adiabatic evolution is practically impossible.

It is worth noticing that we have been dealing with two different definitions of the critical frequency Ω_c: one is the

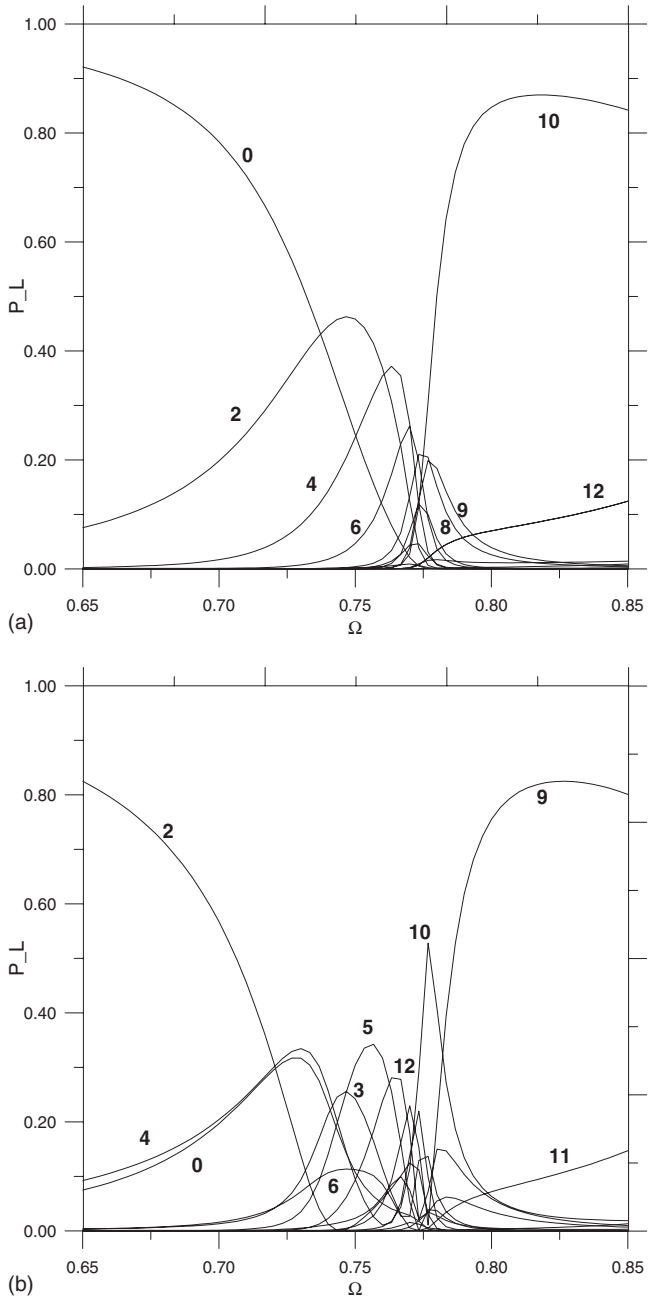

FIG. 10. Weight of the L subspaces in the composition of the GS (upper figure) and the first-excited state (bottom figure) vs Ω. $gN=6$ ($N=10$), $A=0.03$, and $B=0.005$ have been considered.

frequency where the two single-particle occupations equalize ($n_1=n_2$) and the other one is the frequency where the minimum gap between the GS and the first-excited state takes place. Within our numerical precision, both definitions are the same.

V. SIMULATION OF MEASUREMENT

Once we have an accurate representation of the GS at the critical frequency for both cases, with and without parity symmetry breaking, we can simulate measurements during a TOF experiment for an arbitrary large number of atoms

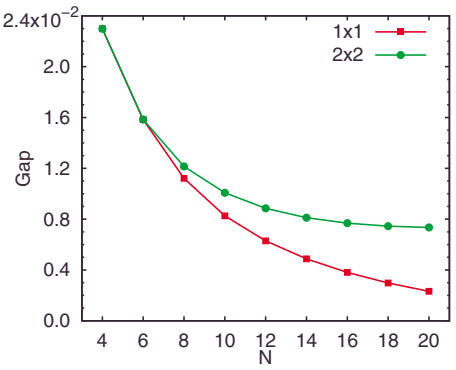

FIG. 11. (Color online) Minimal gap (G_m) between the GS and the first-excited state as a function of N. In the upper curve, only even values of L have been considered (2×2), whereas for the lower curve, all L are included (1×1). $A=0.03$, $B=0$, and $gN=6$ are considered in all cases.

[49]. We assume ballistic expansion, a hypothesis compatible with our LLL condition [60]. We proceed as follows. After solving the eigenvalue equation for the SPDM of the exact GS [see Eqs. (9) and (10)], we get ψ_1 and ψ_2 for the two modes. Then the density distribution of the GS (the two-mode model state) determines the position of the first atom using the following algorithm. A randomly generated position $\vec{r}$ is accepted if $\rho(\vec{r})/\rho_{\max}$ is larger than another randomly generated number u, $0\leq u\leq 1$, or rejected otherwise; $\rho_{\max}$ being the maximum of the density. This first step ends up with the detected position of the first atom: let us call it $\vec{r}_1$. Next we consider the pair-correlation function (PCF) given by $\rho^{(2)}(\vec{r}_1,\vec{r})=\langle \mathrm{GS}|\hat{\Psi}^\dagger(\vec{r}_1)\hat{\Psi}^\dagger(\vec{r})\hat{\Psi}(\vec{r})\hat{\Psi}(\vec{r}_1)|\mathrm{GS}\rangle$ [being $\hat{\Psi}(\vec{r})=\Sigma_l\varphi_l\hat{a}_l$ the field operator] and generate the second position in the same way. By repetition of the procedure N times, finally we get the set of positions of all the N atoms. This sequential algorithm simulates a TOF measurement of a single shot. The procedure is the same in both cases, with or without parity-broken symmetry. However, the main difference is that in the first case ($B\neq 0$), the weights of the components $|n,N-n\rangle$ in $|\mathrm{PB}\rangle$ become negligible for $n>18$, which simplifies the numerical calculation.

Figure 12 shows a set of four shots for $N=10\,000$ atoms with $B=0$; here, the spots represent the positions of the N atoms, whereas in Fig. 13, we show the N-correlation function defined as

$$\rho^{(N)}(\vec{r}_1,\vec{r}_2,\ldots,\vec{r}_{N-1},\vec{r}) \tag{19}$$

related to the four shots of Fig. 12, respectively. The N correlation gives the probability to find the last atom at $\vec{r}$ once the other $N-1$ have fixed positions. For such a large number of atoms we obtain, as a general result, that the j-correlation function is indistinguishable from the $j+1$ one, if $j>100$, namely, the correlation is important only for the first positions. From the sample of four single shots shown in Fig. 12, it is clear that a vortex is produced at random places along the x axis (this axis is preferred due to the particular form of the anisotropic term), with sometimes a slight manifestation of a second vortex, as is the case of the first shot. At odds

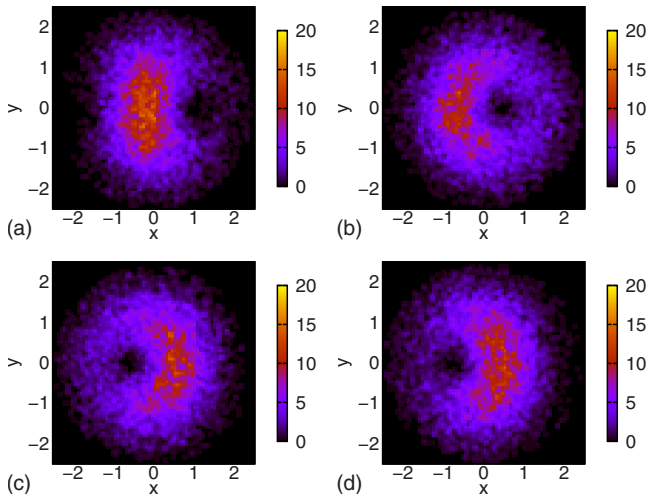

FIG. 12. (Color online) Set of four single shots on the $|\mathrm{ME}\rangle$ state for $N=10\,000$, $A=0.03$, and $B=0$.

with this result, in the case where parity symmetry has been broken (i.e., the last degree of freedom), the GS is projectedonto the most probable option and the vortex always appears at the same place (see Fig. 14) at a negative value of x in our case. This result is again due to our particular choose of the parity-broken term in the Hamiltonian, namely, the vortex would be located at a positive x if

$$V_2(x) = -B\frac{M\omega_\perp^2}{\lambda_\perp}\sum_i^N x_i^3 \tag{20}$$

had been chosen.

We interpret the results in the following way: each image of the system in a single shot (in the case $B=0$, for example) is produced by two ingredients: one is the "intrinsic" nature of the GS which determines the density distributions of the $j \leq N$ successive correlation functions (or equivalently the density of systems with $N-j+1$ particles) and the other is the particular measurement procedure, in our case by a one-by-one detection of the atoms. In other words, the measurement modifies the system and the pictures shown are a combination of the two factors. Different type of experiments detecting particle positions would produce different pictures, coming however from the same GS. However, the differences disappear in the averaged picture given by the density. The experimental mechanism does not modify the mean properties of the system.

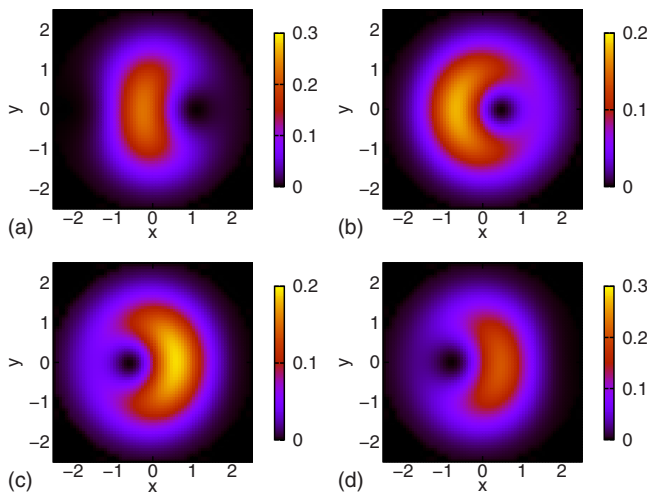

FIG. 13. (Color online) Nth correlation functions of the shots of Fig. 12 [see Eq. (19)].

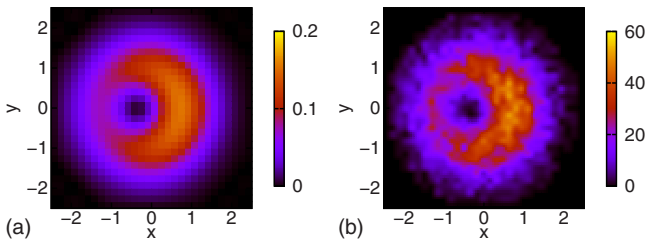

FIG. 14. (Color online) A single shot on the $|\mathrm{PB}\rangle$ state (PB for parity broken) and its Nth correlation function for $N=1000$, $A=0.03$, and $B=0.001$.

According to the result demonstrated in Appendix B, the accumulation of a large number of shots for a macroscopic system reproduces the density. However, an unexpected result is that the density of a system of $N=10\,000$ particles is indistinguishable from that of a reduced N ($N \leq 20$), meaning that some mean properties of macroscopic systems are well captured by the exact results from mesoscopic systems making unnecessary the extrapolation to the thermodynamic limit. This density contains two vortices symmetrically positioned along the x axis. We want to stress that at the level of the exact GS, we proved that the holes that appear in the density are real single-quantized vortices as the phase of ψ_1 changes by 2π around them. If the analysis of the nucleation process would had only the density of the sequence of stationary states for increasing Ω from Ω_0 to Ω_c, as a unique source of information, the conclusion would be that the nucleation of the first vortex is preceded by the presence of two symmetric vortices that move to the center. However, this is nothing else than one possibility among the multiple realizations of the experimental performance.

As a test of our procedure to simulate the TOF experiment, we considered a cat state, artificially created from the $|\mathrm{ME}\rangle$ suppressing all the contributions shown in Eq. (17) except those from $|0,N\rangle$ and $|N,0\rangle$. The result is shown in Fig. 15, which corresponds to the densities of ψ_1 and ψ_2 as expected, with one or two vortices. We obtained only two

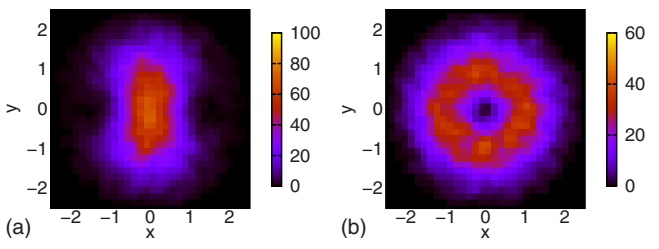

FIG. 15. (Color online) Shots on the cat state.

possibilities, as the system is fully occupying the single particle ψ_1 or ψ_2 and no partial occupations are possible. Thepositions of the noncentered vortices are given by $x=(\sqrt{2}|\frac{\alpha}{\beta}|)^{1/2}\sim 1.5$, where $\psi_1=\alpha\varphi_0+\beta\varphi_2$ in terms of the FD states.

Some experience in the analysis of many-body systems suggests that complementary information can be obtained by the inspection of the PCF [37]. However, the success of such exercise depends strongly on the type of state. Since the meaning of the PCF is the probability of finding an atom at $\vec{r}$ when another one is placed at $\vec{r}_1$, a circular symmetric result means that the system is not correlated, whereas a hole at $\vec{r}_1$ and ordered peaks in special positions means that the position of the atoms is strongly correlated; this is, for example, the case of the Laughlin state, solution of the symmetric Hamiltonian with $L=N(N-1)$ in the region of strong rotation. It is a nondegenerated GS and as a consequence, its density is circular symmetric preserving the symmetry of the Hamiltonian. However, its PCF reveals a strongly correlated Wigner-type structure of N peaks. The reason for the discrepancy between the density and the PCF is that the Laughlin state is a number state with the phase completely undefined (the opposite case of a condensate). It is a linear combination of all possible orientations of the Wigner structure. A measurement that fixes the position of one atom projects the system in a particular orientation, revealing the Wigner structure. In contrast, the GS at Ω_c is the solution of a Hamiltonian that contains a rotating symmetry-breaking term ($A\neq 0$) and has a fixed orientation. The PCF does not provide then extra unknown information if $\vec{r}_1$ is chosen at the maximum of the density.

Finally, we want to mention a speculation. In the case of a system submitted to both types of anisotropy ($A\neq 0$ and $B\neq 0$) and considering in general both signs for the parameter B, the density of the system would contain two vortices in fixed symmetric positions on the x axis. This state is a candidate to experience tunneling between the two single vortex states in agreement with the picture raised by Parke *et al.* [38] as the precursor mechanism for the nucleation.

VI. CONCLUSIONS

We have analyzed in this paper vortex nucleation in mesoscopic 2D Bose superfluid in a rotating trap. The main ingredient of our work is that we have included a weakly anisotropic stirring potential, breaking thus explicitly the axial (rotational) symmetry. The system we consider is well described by the mean-field theory well below "criticality" (with an even condensate wave function) and well above the criticality, with the order parameter being an odd function. This phenomenon involves therefore a discrete parity symmetry breaking in the order parameter. In the critical region, the MF solutions exhibit dynamical instability. The main result of our paper is that the true many-body state in this region is a strongly correlated entangled state involving two macroscopically occupied modes (eigenvectors of the single-particle density matrix). We have characterized this state in various aspects, which can be summarized in more details as follows:

(i) The parity symmetry breaking at the critical frequency manifests itself as dynamical instability within the mean-field framework. It does not prevent, however, the adiabaticity of the nucleation process. The increase of the parity conserving perturbation A notably reduces the necessary period of time to evolve from Ω_0 to Ω_f (for $A=0.1$, $\Delta t\sim 1$ s). This conclusion remains valid even when the number of particles increases. However, a significant value of the parity-breaking perturbation ($B\neq 0$) evidently acts against the adiabaticity. This perturbation leads to an exponential decrease of the energy gap from the GS to the first-excited state.

(ii) The maximally entangled combination of ψ_1 and ψ_2 of the two-mode state, which is a fairly accurate representation of the strongly correlated state at the critical frequency for $B=0$, reveals a single vortex structure randomly located along the x axis in a single shot measurement (with an additional small probability of a pair of, in general, nonsymmetrically located vortices). This is the result of the particular way of measurement mechanism that we consider here; a one-particle-followed-by-another-one detection.

(iii) The function $\rho^{(2)}(\vec{r}_1,\vec{r})$, with $\vec{r}_1$ at one of the peaks of the density on the y axis, does not reveal any hidden structure due to the fact that the system has a fixed orientation and the position of the vortex along the x axis is smeared out by the integration over the positions of the other $N-2$ atoms. This is an intrinsic property of this correlation function. In contrast, $\rho^{(N)}(\vec{r})$ breaks both symmetries, rotational and parity, producing the pictures shown in Fig. 13 typical of a projection mechanism implicit in a single measure [51].

(iv) The state $|\mathrm{ME}\rangle$ becomes a better representation of the exact GS as N increases. It is robust against changes in A for $0\leq A\leq 0.1$. The state $|\mathrm{PB}\rangle$ has zero contribution of $|n,N-n\rangle$ for $n\geq 18$.

(v) The mean properties of the system as those given by the total energy and the density are insensitive to the symmetry-broken mechanism at Ω_c.

(vi) Instability or chaotic behavior of the system in a mean-field calculation can be a signature of the existence of a strongly correlated state whose description lies beyond the mean-field framework.

ACKNOWLEDGMENTS

We acknowledge very fruitful discussions and suggestions from Jean Dalibard. We thank A. Fetter for discussions. We acknowledge Spanish MEC/MINCIN projects TOQATA (Projects No. FIS2008-00784 and No. FIS2007-60350) and QOIT (Consolider Ingenio 2010). M.L. acknowledges ESF/MEC project FERMIX (Project No. FIS2007-29996-E), EU Integrated Project SCALA, EU STREP project NAMEQUAM, ERC Advanced Grant QUAGATUA, and Alexander von Humboldt Foundation.

APPENDIX A

1. Natural orbitals

From the diagonalization of the SPDM, one obtains a new set of single-particle wave functions (SPWF), often called

natural orbitals, and their corresponding annihilation operators given by

$$\psi_i = \sum_{j=0}^{L} \beta_{ij} \varphi_j^{\mathrm{FD}}, \tag{A1}$$

$$\hat{b}_i = \sum_{j=0}^{L} \beta_{ij} \hat{a}_j, \tag{A2}$$

where β_{ij} are real numbers. $\hat{a}_j$ is the operator that annihilates the FD with angular momentum j, $j=0,1,\ldots,L$, being L the largest single-particle angular momentum in the GS $|\Psi_0\rangle$. We have sorted the SPWFs in decreasing order of occupation ($\langle n_i \rangle$) in such a way that $\hat{b}_1$ and $\hat{b}_2$ create the most occupied single particle and the next one, respectively. It is worth to notice that the subindex in $\hat{b}_i$ and ψ_i ($i=1,2,\ldots,L+1$) labels different SPDM eigenstates, whereas the subindex in φ_i^{FD} ($i=0,1,\ldots,L$) means angular momentum.

The representation of a state $|\Psi\rangle$ in terms of the FD functions can be transformed into one in terms of the natural base $\{\psi_i\}$ in the following way. Given a general state

$$|\Psi\rangle = \sum_{k=1}^{dim} \alpha_k |k\rangle_{\mathrm{FD}}, \tag{A3}$$

where $|k\rangle_{\mathrm{FD}}$ is a N-body state expressed in the FD base and dim is the dimension of the space considered, $|k\rangle_{\mathrm{FD}}$ can be expressed as

$$|k\rangle_{\mathrm{FD}} = \frac{1}{\sqrt{\prod_{l=0}^{L} n_{lk}!}} \prod_{j=1}^{N} \hat{a}_{w_{kj}}^{\dagger} |0\rangle, \tag{A4}$$

where n_{lk} is the occupation of FD l in the state $|k\rangle_{\mathrm{FD}}$ and w_{kj} is the angular momentum of each particle in the state $|k\rangle_{\mathrm{FD}}$. Using Eqs. (A2) and (A4) in Eq. (A3),

$$|\Psi\rangle = \sum_{k=1}^{dim} \frac{\alpha_k}{\sqrt{\prod_{l=0}^{L} n_{lk}!}} \prod_{j=1}^{N} \sum_{i=1}^{L+1} \beta_{i,w_{kj}} \hat{b}_i^{\dagger} |0\rangle, \tag{A5}$$

where we have used the orthogonality properties of the β matrix $\{\beta_{ij}\}^{-1} = \{\beta_{ij}\}^{T} = \{\beta_{ji}\}$.

2. Overlap

The ME state is a combination of states $|n, N-n, 0, \ldots\rangle_{\mathrm{SPDM}}$, $n \in$ even, with the same weight, where n is the occupation of the most occupied SPWF and $N-n$ the occupation of the next one. At Ω_c, the first natural orbit is a combination of SPWF with angular momenta $m=0$ and $m=2$, $\psi_1^{\mathrm{SPDM}} = c\varphi_0^{\mathrm{FD}} + d\varphi_2^{\mathrm{FD}}$, with $d = -\sqrt{1-c^2}$ and the second one is equal to the FD with angular momentum $m=1$, $\psi_2^{\mathrm{SPDM}} = \varphi_1^{\mathrm{FD}}$. Then, each state can be expressed in the FD bases as

$$\begin{aligned} &|n, N-n, 0, \ldots, 0\rangle_{\mathrm{SPDM}} \\ &= \frac{(c\hat{a}_0^{\dagger} + d\hat{a}_2^{\dagger})^n (\hat{a}_1^{\dagger})^{N-n}}{\sqrt{n!\,(N-n)!}} |0\rangle \\ &= \sum_{i=0}^{n} \binom{n}{i} \frac{(c\hat{a}_0^{\dagger})^{n-i} (d\hat{a}_2^{\dagger})^i}{\sqrt{n!}} |0, N-n, 0, \ldots, 0\rangle_{\mathrm{FD}} \\ &= \sum_{i=0}^{n} \sqrt{\binom{n}{i}} c^{n-i} d^i |n-i, N-n, i, 0, \ldots, 0\rangle_{\mathrm{FD}}. \end{aligned} \tag{A6}$$

Projecting each of these states on the GS obtained from exact diagonalization $|\mathrm{GS}\rangle = \Sigma_{i_0, i_1, \ldots, i_L} \alpha_{i_0, i_1, \ldots, i_L} |i_0, i_1, \ldots, i_L\rangle_{\mathrm{FD}}$, summing over all the states $|n, N-n, 0, \ldots\rangle_{\mathrm{SPDM}}$, $n \in$ even, and finally multiplying by the normalization constant $1/\sqrt{N/2+1}$, we obtain the overlap expressed in the simple form

$$|\langle \mathrm{GS} | \mathrm{ME} \rangle| = \frac{1}{\sqrt{N/2+1}} \left| \sum_{\substack{n=0 \\ n \in \mathrm{even}}}^{N} \sum_{i=0}^{n} \sqrt{\binom{n}{i}} c^{n-i} d^i \alpha_{n-i, N-n, i, 0, \ldots, 0} \right|, \tag{A7}$$

which measures the suitability of $|\mathrm{ME}\rangle$ as an approximation of the GS.

APPENDIX B

Density

The superposition of the data coming from a large number of single shots reproduces the density of a system in a state $|\Psi\rangle$, as can be shown in what follows. The probability to find a particle at the position $\mathbf{r}$ after k particles have been detected is given by the function ($k \leq N-1$, N the number of particles)

$$\begin{aligned} \rho^{(k+1)}(\mathbf{r_1}, \mathbf{r_2}, \ldots, \mathbf{r_k}, \mathbf{r}) = &\langle \hat{\Psi}^{\dagger}(\mathbf{r_1}) \hat{\Psi}^{\dagger}(\mathbf{r_2}) \cdots \hat{\Psi}^{\dagger}(\mathbf{r_k}) \hat{\Psi}^{\dagger}(\mathbf{r}) \\ &\times \hat{\Psi}(\mathbf{r}) \hat{\Psi}(\mathbf{r_k}) \cdots \hat{\Psi}(\mathbf{r_2}) \hat{\Psi}(\mathbf{r_1}) \rangle, \end{aligned} \tag{B1}$$

where the expected value is in the state Ψ and $\hat{\Psi}(\mathbf{r_k}) = \Sigma_i \varphi_i(\mathbf{r_k}) \hat{a}_i$ is the field operator. Using the commutation relations of the creation and annihilation operators and the ortogonormalization of the set $\{\varphi_i(\mathbf{r_k})\}$, we can deduce the general relations

$$\int_{\mathbf{r_1} \in \mathbb{R}^2} \rho^{(2)}(\mathbf{r_1}, \mathbf{r}) d\mathbf{r_1} = (N-1)\rho(\mathbf{r}), \tag{B2}$$

$$\int_{\mathbf{r_1} \in \mathbb{R}^2} \int_{\mathbf{r_2} \in \mathbb{R}^2} \rho^{(3)}(\mathbf{r_1}, \mathbf{r_2}, \mathbf{r}) d\mathbf{r_1} d\mathbf{r_2} = (N-2)(N-1)\rho(\mathbf{r}), \tag{B3}$$

$$\vdots \tag{B4}$$

$$\int_{\mathbf{r_1}\in\mathbb{R}^2}\int_{\mathbf{r_2}\in\mathbb{R}^2}\cdots\int_{\mathbf{r_{N-1}}\in\mathbb{R}^2}\rho^{(N)}(\mathbf{r_1},\mathbf{r_2},\ldots,\mathbf{r_{N-1}},\mathbf{r})\times d\mathbf{r_1}d\mathbf{r_2}\cdots d\mathbf{r_{N-1}} = (N-1)!\,\rho(\mathbf{r}). \tag{B5}$$

We could use any of them to recover the density, however, the last is the one that fits our simulation. To model the experiment, we have defined a grid in the *xy* plane and we count the number of times that we detect a particle at each site of the grid. On the other hand, if we interpret the multiple integral of Eq. (B5) as a multiple summation on a large number of different configurations $\{\mathbf{r_1},\mathbf{r_2},\ldots,\mathbf{r_{N-1}},\mathbf{r}\}$ on the discretized grid, keeping $\mathbf{r}$ fixed, then we can make the connection since the histogram obtained after a large number of shots is nothing else than, aside of a constant number, the probability to find a particle at $\mathbf{r}$ when the other $N-1$ have visited all the possible configurations, which is the meaning of the correlation function $\rho^{(N)}$ in the left-hand side of Eq. (B5). More than that, the summation over the $\rho^{(N)}$ functions is not arbitrary. It contains the information of the structure of the state Ψ as is the case in the simulation. It can be easily proved, for example, in the case of the pair-correlation function that can be rewritten as

$$\rho^{(2)}(\mathbf{r_1},\mathbf{r}) = \langle V_0|\hat{\Psi}^\dagger(\mathbf{r_1})\hat{\Psi}^\dagger(\mathbf{r})\hat{\Psi}(\mathbf{r})\hat{\Psi}(\mathbf{r_1})|V_0\rangle = \rho(\mathbf{r_1})\langle V_1|\hat{\Psi}^\dagger(\mathbf{r})\hat{\Psi}(\mathbf{r})|V_1\rangle, \tag{B6}$$

where

$$|V_1\rangle = \frac{\hat{\Psi}(\mathbf{r_1})|V_0\rangle}{\sqrt{\rho(\mathbf{r_1})}} \tag{B7}$$

is a system with $N-1$ particles and $|V_0\rangle$ is the initial state $|\Psi\rangle$. Or in other words, the probability to find a particle at $\mathbf{r}$ when other is located at $\mathbf{r_1}$ depends on the probability to have a particle at $\mathbf{r_1}$ in the state Ψ. This completes our assertion.

[1] S.-K. Ma, *Statistical Mechanics* (World Scientific, Singapore, 1998).
[2] R. K. Pathria, *Statistical Mechanics* (Butterworth-Heinemann, Oxford, 1996).
[3] P. Weiss, J. Phys. Theor. Appl. **6**, 661 (1907).
[4] K. R. Wilson, Rev. Mod. Phys. **47**, 773 (1975).
[5] D. J. Amit, *Field Theory, the Renormalization Group, and Critical Phenomena* (McGraw-Hill International Book Co., London, 1978).
[6] L. Pitaevskii and S. Stringari, *Bose-Einstein Condensation* (Oxford University Press, Oxford, 2003).
[7] S. Sachdev, *Quantum Phase Transitions* (Cambridge University Press, Oxford, 2001).
[8] A. Griffin, *Excitations in a Bose-Condensed Liquid*, Cambridge Studies in Low Temperature Physics (Cambridge University Press, Cambridge, England, 1993).
[9] A. L. Fetter, Rev. Mod. Phys. **81**, 647 (2009).
[10] N. R. Cooper, Adv. Phys. **57**, 539 (2008).
[11] L. P. Pitaevskii, Sov. Phys. JETP **13**, 451 (1961).
[12] E. P. Gross, Nuovo Cimento **20**, 454 (1961).
[13] S. Stringari, Phys. Rev. Lett. **82**, 4371 (1999).
[14] M. R. Matthews, B. P. Anderson, P. C. Haljan, D. S. Hall, C. E. Wieman, and E. A. Cornell, Phys. Rev. Lett. **83**, 2498 (1999).
[15] Ł. Dobrek, M. Gajda, M. Lewenstein, K. Sengstock, G. Birkl, and W. Ertmer, Phys. Rev. A **60**, R3381 (1999).
[16] K. W. Madison, F. Chevy, W. Wohlleben, and J. Dalibard, Phys. Rev. Lett. **84**, 806 (2000).
[17] F. Chevy, K. W. Madison, and J. Dalibard, Phys. Rev. Lett. **85**, 2223 (2000).
[18] K. W. Madison, F. Chevy, V. Bretin, and J. Dalibard, Phys. Rev. Lett. **86**, 4443 (2001).
[19] C. Raman, J. R. Abo-Shaeer, J. M. Vogels, K. Xu, and W. Ketterle, Phys. Rev. Lett. **87**, 210402 (2001).
[20] J. R. Abo-Shaeer, C. Raman, and W. Ketterle, Phys. Rev. Lett. **88**, 070409 (2002).
[21] P. C. Haljan, I. Coddington, P. Engels, and E. A. Cornell, Phys. Rev. Lett. **87**, 210403 (2001).
[22] E. Hodby, G. Hechenblaikner, S. A. Hopkins, O. M. Maragò, and C. J. Foot, Phys. Rev. Lett. **88**, 010405 (2001).
[23] I. Bloch, J. Dalibard, and W. Zwerger, Rev. Mod. Phys. **80**, 885 (2008).
[24] G. Birkl and J. Fortagh, Laser Photonics Rev. **1**, 12 (2007).
[25] E. Sarajlic, N. Gemelke, S.-W. Chiow, S. Herrman, H. Müller, and S. Chu, in *Pushing the Frontiers of Atomic Physics, Proceedings of the XXI International Conference on Atomic Physics*, edited by R. Ct, P. L. Gould, M. Razman, and W. W. Smith (World Scientific, New Jersey, 2009), p. 34.
[26] N. K. Wilkin and J. M. F. Gunn, Phys. Rev. Lett. **84**, 6 (2000).
[27] D. Yoshioka, *The Quantum Hall Effect* (Springer, Heidelberg, 2002).
[28] D. L. Feder, C. W. Clark, and B. I. Schneider, Phys. Rev. A **61**, 011601(R) (1999).
[29] S. Sinha and Y. Castin, Phys. Rev. Lett. **87**, 190402 (2001).
[30] K. Kasamatsu, M. Tsubota, and M. Ueda, Phys. Rev. A **67**, 033610 (2003).
[31] D. A. Butts and D. S. Rokhsar, Nature (London) **397**, 327 (1999).
[32] G. F. Bertsch and T. Papenbrock, Phys. Rev. Lett. **83**, 5412 (1999).
[33] R. A. Smith and N. K. Wilkin, Phys. Rev. A **62**, 061602(R) (2000).
[34] A. D. Jackson and G. M. Kavoulakis, Phys. Rev. Lett. **85**, 2854 (2000).
[35] D. Dagnino, N. Barberán, K. Osterloh, A. Riera, and M. Lewenstein, Phys. Rev. A **76**, 013625 (2007).
[36] N. Barberán, M. Lewenstein, K. Osterloh, and D. Dagnino, Phys. Rev. A **73**, 063623 (2006).
[37] I. Romanovsky, C. Yannouleas, and U. Landman, Phys. Rev. A **78**, 011606(R) (2008).
[38] M. I. Parke, N. K. Wilkin, J. M. F. Gunn, and A. Bourne, Phys. Rev. Lett. **101**, 110401 (2008).
[39] A. G. Morris and D. L. Feder, Phys. Rev. A **74**, 033605

(2006); A. L. Fetter, *ibid.* **75**, 013620 (2007).
[40] R. Seiringer, e-print arXiv:0801.0427.
[41] E. H. Lieb, R. Seiringer, and J. Yngvason, Phys. Rev. A **79**, 063626 (2009).
[42] P. Rosenbusch, D. S. Petrov, S. Sinha, F. Chevy, V. Bretin, Y. Castin, G. Shlyapnikov, and J. Dalibard, Phys. Rev. Lett. **88**, 250403 (2002).
[43] G. Andrelczyk, M. Brewczyk, Ł. Dobrek, M. Gajda, and M. Lewenstein, Phys. Rev. A **64**, 043601 (2001).
[44] L. J. Garay, J. R. Anglin, J. I. Cirac, and P. Zoller, Phys. Rev. Lett. **85**, 4643 (2000).
[45] D. Dagnino, N. Barberan, M. Lewenstein, and J. Dalibard, Nat. Phys. **5**, 431 (2009).
[46] M. Ueda and T. Nakajima, Phys. Rev. A **73**, 043603 (2006).
[47] A. Nunnenkamp, A. M. Rey, and K. Burnett, Phys. Rev. A **77**, 023622 (2008).
[48] C. Weiss and N. Teichmann, Phys. Rev. Lett. **100**, 140408 (2008).
[49] J. Javanainen and S. M. Yoo, Phys. Rev. Lett. **76**, 161 (1996).
[50] Y. Castin and J. Dalibard, Phys. Rev. A **55**, 4330 (1997).
[51] W. J. Mullin, R. Krotkov, and F. Lalöe, Am. J. Phys. **74**, 880 (2006).
[52] W. S. Bakr, J. I. Gillen, A. Peng, S. Foelling, and M. Greiner, e-print arXiv:0908.0174.
[53] I. Bloch (private communication).
[54] L. Jacak, P. Hawrylak, and A. Wojs, *Quantum Dots* (Springer-Verlag, Berlin, 1997).
[55] O. Penrose and L. Onsager, Phys. Rev. **104**, 576 (1956).
[56] H. Saito and M. Ueda, Phys. Rev. Lett. **93**, 220402 (2004).
[57] J. I. Cirac, M. Lewenstein, K. Mølmer, and P. Zoller, Phys. Rev. A **57**, 1208 (1998).
[58] K. Eckert, J. Schliemann, D. Bruß, and M. Lewenstein, Ann. Phys. **299**, 88 (2002).
[59] P. Zanardi, Phys. Rev. A **65**, 042101 (2002).
[60] N. Read and N. R. Cooper, Phys. Rev. A **68**, 035601 (2003).
[61] E. M. Wright (unpublished).